Journal of Fluids and Structures 28 (2012) 56–71

Contents lists available at SciVerse ScienceDirect

Journal of Fluids and Structures

journal homepage: www.elsevier.com/locate/jfs

Experiments and computations of a loosely supported tube in a rigid bundle subjected to single-phase flow

Philippe Piteau [a,*], Xavier Delaune [a], Jose Antunes [b], Laurent Borsoi [a]

[a] Commissariat à l'Energie Atomique et aux Energies Alternatives, Laboratoire d'Études de Dynamique CEA, DEN, DM2S, SEMT, DYN, F-91191 Gif-sur-Yvette, France

[b] Instituto Tecnológico e Nuclear, Applied Dynamics Laboratory, ITN/ADL, 2686 Sacavem, Portugal

ARTICLE INFO

Article history:
Received 18 May 2010
Accepted 8 August 2011
Available online 19 October 2011

Keywords:
Flow induced vibration
Loosely supported tube
Fluidelastic
Turbulence
Nonlinear dynamics

ABSTRACT

In this paper the problem of computing the nonlinear vibro-impact responses of loosely supported heat-exchanger tubes subjected to fluidelastic coupling forces, as well as to the turbulence excitation from transverse flows, is addressed. Emphasis is on the fluidelastic modeling within a time domain nonlinear framework, as well as on the stabilizing effect of impacts on the fluidelastic coupling forces. Theoretical computations of the linear and vibro-impacting regimes of a flow-excited flexible cantilever test tube, within a rigid 3×5 square bundle, are based on the experimentally identified fluidelastic coupling force coefficients and turbulence spectrum. Computations are then compared with the experimental vibratory responses, enabling a full validation of the modeling approach. Furthermore, interesting conclusions are drawn, concerning (a) the energy balance between sources and sinks, for a vibro-impacting tube subjected to fluidelastic forces and (b) the dependence of the vibration response frequency on impacts at the loose supports, and their effect on the nonlinear restabilization of fluidelastically unstable tubes. Details on the following aspects are reported in the paper: (1) numerical modeling of the fluidelastic coupling forces for the time domain computations; (2) experimental identification of the fluidelastic coupling coefficients; (3) computations and experiments of both linear and vibro-impacting responses under the combined action of turbulence and fluidelastic coupling and (4) energy aspects of the vibro-impacting fluidelastically coupled tube responses.

1. Introduction

It is well known that heat-exchanger tube bundles are subjected to fluidelastic coupling forces, which depend on the bundle geometry, fluid nature (single-phase or two-phase) and on the fluid velocity. Reliable modeling of such coupling forces is very difficult, therefore several authors since the pioneering work of Tanaka and Takahara (1981) have attempted to measure the fluidelastic linearized stiffness and damping coefficients as a function of the flow reduced velocity (or reduced frequency), for specific fluid mixtures and bundle geometries, in order to link the dynamical behavior of the flow-coupled tube bundle with simpler stability criteria such as those provided by Connors (1970) and many others since, see the relevant work by Chen et al. (1998). For instance, recent experiments on tube bundles subjected to fluid-elastic forces were performed under two-phase flows by Mitra et al. (2009). Other experimental work has also been offered, focusing on bundles of tubes with non-circular cross-section, see Inada et al. (2003).

* Corresponding author. Tel.: +33 1 69 08 20 88; fax: +33 1 69 08 76 19.
E-mail address: Philippe.Piteau@cea.fr (P. Piteau).

0889-9746/$ - see front matter © 2011 Elsevier Ltd. All rights reserved.
doi:10.1016/j.jfluidstructs.2011.08.007

Nomenclature

A	area of the tube cross-section
C_d	dimensionless damping coupling coefficient
C_k	dimensionless stiffness coupling coefficient
C_m	dimensionless inertia coupling coefficient
$[\mathcal{D}_S]$	structural modal damping matrix
$[\mathcal{D}_F(t)]$	fluidelastic modal damping matrix
D	tube diameter
D_F	fluidelastic damping coupling coefficient
E	Young's modulus of the tube
f	frequency
$\bar{f}_r$	response frequency estimate
$f_R = \bar{f}_r D/V$	reduced frequency
$f(x,t)$	total excitation force field
$f_F(x,t)$	fluidelastic coupling force field
$f_T(x,t)$	turbulence force field
$f_C(x,t)$	contact/impact force field
$F_C(t)$	contact/impact force at support x_C
$F_n(t)$	total modal force (mode n)
$F_n^F(t)$	fluidelastic component of the modal force
$F_n^T(t)$	turbulence component of the modal force
$F_n^C(t)$	contact/impact component of the modal force
$\{\mathcal{F}(t)\}$	vector of modal forces
I	moment of inertia of the tube cross-section
K_F	fluidelastic stiffness coupling coefficient
K_C	tube/support contact stiffness
$[\mathcal{K}_S]$	structural modal stiffness matrix
$[\mathcal{K}_F(t)]$	fluidelastic modal stiffness matrix
L	tube length
M_F	fluidelastic inertia coupling coefficient
m_n	modal mass (mode n)
$[\mathcal{M}_S]$	structural modal mass matrix
$[\mathcal{M}_F]$	fluidelastic modal mass matrix
$n=1,2,\ldots,N$	modal index
$q_n(t)$	modal response (mode n)
$\{Q(t)\}$	vector of modal amplitudes
t	time
T	total simulation duration
V	transverse pitch flow velocity
$V_R = V/\bar{f}_r D$	reduced velocity
x	location along the tube
$Y(x,t)$	flexural tube response
δ_c	support gap
ζ_n	modal damping (mode n)
η	tube viscous dissipation coefficient
ρ	mass density of the tube
σ	rms value of the tube displacement
$\phi_n(x)$	modeshape (mode n)
$[\Phi]_e(f_R)$	dimensionless equivalent spectrum
ω_n	modal circular frequency (mode n)

When looking at the loosely supported tubes of real life components, time domain nonlinear computing methods have been developed by several research groups for the predictive analysis of vibro-impacting flow-excited tubes. As far as fluidelastic forces are concerned, the first attempt to include them in the computations – along with the ever-present turbulent excitation – was achieved by Axisa et al. (1988), who used a flow velocity dependent negative damping coefficient on the linearly unstable mode, deduced from Connors' formulation. This pioneering approach was followed by others, along similar lines, see Fricker (1992), for instance, who additionally corrected the computation of the fluidelastic coupling effect using an estimate of the actual response frequency instead of the modal frequency of the unstable mode. Since then, others have tackled this problem in a more sophisticated manner, by directly incorporating in their computer programs models of the fluidelastic coupling forces, see Rao et al. (1992), Sauvé (1996), Hadj-Sadok et al. (1997) and Hassan and Hayder (2008).

Nevertheless, it is still debatable how realistic are the strongly nonlinear and unsteady vibro-impact regimes produced by computations, which stem from fluidelastic coefficients obtained under linear and steady conditions. Furthermore, it is well known that, when loosely supported tubes become linearly unstable, impacting produces an increase of the actual tube response frequencies, which somehow tend to restabilize the system. Because of these difficulties, there is urgency in confronting the rationale of such computational approach with actual experimental results. Such is the aim of the present paper. Vibro-impact controlled experiments under linearly unstable conditions were performed in the past by Antunes et al. (1992) and Vento et al. (1992). However, in their work, the tube instability was created by an electro-mechanical feedback controlled system, such that the "fluidelastic" coupling stiffness coefficient was nil and the coupling damping coefficient was independent of the system response frequency. A different exploratory angle has been investigated by Mureithi et al. (1996), who performed fractal dimension computations on pseudo-phase space reconstructions from the flow-induced responses of a multi-supported tube, in order to distinguish the (post Hopf bifurcation) fluidelastically unstable chaotic vibro-impact responses from the randomness due to turbulence. Although all these former experiments produced interesting qualitative results, in the case of real flow-excited tube bundles, these are unrealistic over-simplifications. The authors believe that carefully controlled experiments of loosely supported tubes subjected to fluidelastic coupling forces are needed, in view of validating the current computational approaches for such systems, as well as to increase our physical understanding of the stabilizing mechanisms provided by the impact dynamics.

It should be emphasized that providing results, which directly apply to real life components, is secondary in the present paper. As stated before, the main motivation in this work was to experimentally validate a computational methodology for tubes subjected to the combined actions of turbulence and fluidelastic forces, the authors' interest being to study a system governed by as few fluidelastic parameters as possible. Actually, the chosen configuration is governed by only two flow dependent coefficients, instead of two matrices of them, as would be the case if a fully flexible bundle had been chosen. Obviously, because the system studied here is constrained to planar motions leading to normal impact forces only, friction

and wear related effects, which would be unavoidable in tubes with two-dimensional vibrations will not be addressed. The authors are well aware of this limitation in the present work, however such realistic aspects were not of prime interest here.

Based on the active vibration control method proposed by Caillaud et al. (1999, 2000, 2003), new experiments were recently performed at CEA-Saclay on the same experimental rig, consisting of a flexible tube (vibrating along the lift direction) inserted in a rigid square bundle. First, the linearized fluidelastic coupling coefficients, as well as the turbulence excitation, were identified for a significant range of reduced velocity, in water cross-flow. Then, nonlinear experiments were performed under the same conditions after installing an instrumented loose support in the rig, from which both the tube responses and the impact forces were measured.

These experimental results are compared with the linear and vibro-impact numerically simulated responses obtained from a time-domain computer program, where the experimentally identified linear fluidelastic coupling coefficients were implemented. A delicate aspect of such implementation is the real time estimation of a representative instantaneous response frequency of the vibro-impacting tube, which is needed because the coupling coefficients depend on the "instantaneous" reduced frequency. Several techniques for such frequency tracking are mentioned, and the authors propose a new one for near "real time" estimation of the nonlinear tube response frequency. Then a satisfying comparison between the experimental results and nonlinear computed predictions is produced, which validates the authors' current computational approach for linearly unstable loosely supported tubes. On the other hand, computations show the energy aspects behind the nonlinear stabilization of fluidelastically unstable tubes, as well as their relation with the increase in the tube response frequency due to impacts.

2. Numerical modeling of the flow excited loosely supported tube

2.1. Time domain computation of the nonlinear dynamics

As discussed by Axisa et al. (1988) and De Araújo et al. (1998), the simple Bernoulli–Euler theory for flexural vibrations proved to be adequate for impact identification. Therefore, assuming a viscous damping model, the small amplitude flexural response of a tube with constant cross-sectional properties is described by the differential equation:

$$\rho A\frac{\partial^2 Y}{\partial t^2}+\eta\frac{\partial Y}{\partial t}+EI\frac{\partial^4 Y}{\partial x^4}=f(x,t)=f_F(x,t)+f_T(x,t)+f_C(x,t), \tag{1}$$

where $f(x,t)$ is the total external excitation field and $Y(x,t)$ is the tube transverse flexural response, E is Young's modulus and ρ is the mass density of the tube, A is the area and I is the moment of inertia of the cross-section, while η is a viscous dissipation coefficient. The total excitation field in Eq. (1) stems from the fluidelastic coupling forces $f_F(x,t)$, the turbulence forces $f_T(x,t)$ and the contact/impact forces $f_C(x,t)=\sum_C F_C(t)\,\delta(x-x_C)$ located at the loose supports x_C.

As amply discussed by Axisa et al. (1988) and Antunes et al. (1990), the vibro-impact nonlinear computations under flow excitation may be performed in an effective manner by projecting Eq. (1) on the tube unconstrained modes $\phi_n(x)$. Then, the following discretized modal equations are obtained:

$$m_n\ddot{q}_n+2m_n\omega_n\zeta_n\dot{q}_n+m_n\omega_n^2 q_n=F_n(t)=F_n^F(t)+F_n^T(t)+F_n^C(t), \tag{2}$$

in terms of the modal amplitudes $q_n(t)$ and its derivatives, with the modal masses m_n, frequencies ω_n and damping values ζ_n, $n=1,2,\ldots,N$. In matrix notation:

$$[\mathcal{M}_S]\{\ddot{Q}\}+[\mathcal{D}_S]\{\dot{Q}\}+[\mathcal{K}_S]\{Q\}=\{\mathcal{F}^F(t)\}+\{\mathcal{F}^T(t)\}+\{\mathcal{F}^C(t)\}. \tag{3}$$

The total modal forces $F_n(t)$ in the right hand side of Eq. (2) are computed from the modal projections of the fluidelastic, turbulence and contact/impact terms:

$$F_n^F(t)=\int_0^L f_F(x,t)\varphi_n(x)dx;\quad F_n^T(t)=\int_0^L f_T(x,t)\varphi_n(x)dx;$$
$$F_n^C(t)=\int_0^L\left(\sum_C F_C(t)\delta(x-x_C)\right)\varphi_n(x)dx=\sum_C F_C(t)\varphi_n(x_C), \tag{4}$$

where L is the tube length.

The physical motions may be computed from the modal responses at any time and location, by modal superposition:

$$Y(x,t)=\sum_{n=1}^{N}\varphi_n(x)q_n(t), \tag{5}$$

and similarly for all time derivatives. The computational truncation index N of the modal basis is chosen accounting for the frequency ranges excited by the various sources of excitation.

2.2. Fluidelastic coupling forces

In their recent work, Hassan and Hayder (2008) developed a direct implementation of the Lever and Weaver (1982) model to compute the fluidelastic coupling forces, which does not require the knowledge of the instantaneous tube response frequency. However, the most common approach – and the only available one if one wishes to use experimentally identified force data – is to express the linearized fluidelastic forces $f_F(x,t)$ in terms of coupling coefficients M_F, D_F and K_F, which in general depend on V_R. Then, the fluidelastic force reads

$$f_F(x,t) = -M_F\ddot{Y}(x,t) - D_F(V_R(x,t))\dot{Y}(x,t) - K_F(V_R(x,t))Y(x,t), \tag{6}$$

where only the fluid inertia coupling coefficient is assumed not dependent on the reduced flow velocity $V_R(x,t)$, here defined as

$$V_R(x,t) = V(x)/[\bar{f}_r(x,t)D], \tag{7}$$

with $\bar{f}_r(x,t)$ an estimate of the "instantaneous" local response frequency of the nonlinearly vibrating tube. It is convenient to define dimensionless coupling coefficients, which may be presented in the following form (Tanaka and Takahara, 1981; Granger et al., 1993):

$$C_m = \frac{M_F}{(1/2)\rho D^2 L}; \quad C_d(V_R) = \frac{D_F(V_R)}{(1/2)\rho DVL}; \quad C_k(V_R) = \frac{K_F(V_R)}{(1/2)\rho V^2 L}. \tag{8}$$

Then, after modal projections, the fluidelastic force field (6) leads to the following modal forces:

$$\{\mathcal{F}^F(t)\} = -[\mathcal{M}_F]\{\ddot{Q}\} - [\mathcal{D}_F(V_R)]\{\dot{Q}\} - [\mathcal{K}_F(V_R)]\{Q\}, \tag{9}$$

where the terms of the modal fluidelastic coupling matrices are computed as

$$\begin{aligned} m^F_{nm} &= \int_0^L M_F\varphi_n(x)\varphi_m(x)dx, \\ d^F_{nm}(V_R) &= \int_0^L D_F(V_R(x,t))\varphi_n(x)\varphi_m(x)dx, \\ k^F_{nm}(V_R) &= \int_0^L K_F(V_R(x,t))\varphi_n(x)\varphi_m(x)dx. \end{aligned} \tag{10}$$

From (3) and (9) one can obtain the changes in the system modal properties, due to the fluidelastic coupling, as a function of the flow velocity. In the frequency domain:

$$[\lambda^2([\mathcal{M}_S]+[\mathcal{M}_F]) + \lambda([\mathcal{D}_S]+[\mathcal{D}_F(V_R)]) + ([\mathcal{K}_S]+[\mathcal{K}_F(V_R)])]\{\overline{Q}\} = \{0\}, \tag{11}$$

where $\lambda_n(V_R) = \sigma_n(V_R) \pm i\ \nu_n(V_R)$ are the complex eigenvalues of the flow coupled system, which are related to the modal properties as

$$\omega_n(V_R) = \sqrt{\sigma_n^2(V_R) + \nu_n^2(V_R)}; \quad \zeta_n(V_R) = -(\sigma_n(V_R))/(\omega_n(V_R)). \tag{12}$$

Notice that, because the modal coupling coefficients depend on the response frequencies encapsulated in V_R, the eigencomputation (11) should be performed in iterative manner.

2.3. Turbulence forces

Modeling of the turbulence excitation $f_T(x,t)$ by the transverse flow is based on the general theory developed by Axisa et al. (1990). Then, generation of time domain realizations of the turbulence forces is achieved using the efficient method recently proposed by Antunes et al. (2008, 2009).

Accordingly, the authors start from the measured equivalent reference spectrum $[\Phi]_e(f_R)$ of the turbulence forces per unit tube length, where $f_R = \bar{f}_r D/V$ is the reduced frequency. Then, a set of uncorrelated random point forces is applied along the tube, using a computation technique, which preserves the spectral content as well as the space correlation of the original turbulence force field, accounting for the flow velocity profile. See the aforementioned references for details.

2.4. Contact forces at loose supports

A single nonlinear loose support is assumed in this paper, in accordance with the experimental rig. The contact force $F_C(t)$ is computed in an explicit manner from the system response, at each time step, using the following penalty formulation:

$$F_C(t) = \begin{cases} -K_C[Y(x_C,t) - \delta_C] & \text{if } |Y(x_C,t)| \geq |\delta_C|, \\ 0 & \text{if } |Y(x_C,t)| < |\delta_C|, \end{cases} \tag{13}$$

where K_C is a suitable value for the contact stiffness at the support, which is pragmatically adjusted such that the numerical simulations reproduce the elementary contact duration of the experimental impacts. Contact models more refined than this

simple point model have been developed by several authors, see in particular Hassan et al. (2005), nevertheless for the purposes of the present study the straightforward approach expressed in Eq. (13) is adequate. Because the tube motions studied in this paper are planar and the corresponding impacts only display a radial component, there is no need to implement a friction contact model (Antunes et al., 1990).

One may notice, from Eqs. (5) and (13), that the tube/support interaction couples the system unconstrained modes. Indeed, during contact, one obtains

$$F_C(t) = -K_C\left[\sum_{n=1}^{N}\varphi_n(x_C)q_n(t) - \delta_C\right], \tag{14}$$

which clearly shows that the tube/support impacts couple all modes, redistributing the modal energies.

2.5. Quasi-instantaneous response frequency

As stated earlier, an estimate of some representative "instantaneous" response frequency $\bar{f}_r(x,t)$ of the impacting tube is needed when performing time domain numerical simulations, because the fluidelastic coefficients depend on the reduced velocity $V_R(x,t)$. Several methods have been used by researchers in this field, including straight time domain evaluations of the zero crossing frequency or a time window adaptation of Rice's formula (1945):

$$\bar{f}_r(x,t) = \frac{1}{2\pi}\frac{\sigma_{\dot{Y}}(x,t;\tau)}{\sigma_Y(x,t;\tau)}, \tag{15}$$

where $\sigma_Y(x,t;\tau)$ is the RMS value of the vibratory displacement at location x, computed within the updated time window of size τ, e.g. $[t-\tau,t]$, and $\sigma_{\dot{Y}}(x,t;\tau)$ is the RMS value of the corresponding velocity. An equivalent measure may be defined in the frequency domain, using the autospectrum S_{YY} computed from the signal time windowed within τ (Au-Yang, 2002):

$$\bar{f}_r(x,t) = \frac{\int_0^{f_{\max}} f^2 S_{YY}(x,f;\tau)df}{\int_0^{f_{\max}} S_{YY}(x,f;\tau)df}. \tag{16}$$

Other methods can be adapted from various fields involving non-stationary signals, for instance in voice and music analysis, where several time domain and frequency-domain techniques are used for the frequency (pitch) tracking in speech and singing, including auto-correlation, auto-regressive, maximum likelihood, adaptive filtering and cepstral techniques, see Boashash (1992) or Pachet and Briot (2004) for reviews. Even so, for the computations of the present study, the authors have developed a simple estimation method, which proved to be efficient and reliable enough. It is based on a least-squares fit of the parameters of an "equivalent" 1-dof oscillator, to the nonlinear computed responses within the sliding time window τ:

$$\begin{Bmatrix} \ddot{Y}(x,t) \\ \vdots \\ \ddot{Y}(x,t-\tau) \end{Bmatrix} + A\begin{Bmatrix} \dot{Y}(x,t) \\ \vdots \\ \dot{Y}(x,t-\tau) \end{Bmatrix} + B\begin{Bmatrix} Y(x,t) \\ \vdots \\ Y(x,t-\tau) \end{Bmatrix} = \begin{Bmatrix} 0 \\ \vdots \\ 0 \end{Bmatrix}, \tag{17}$$

hence

$$\begin{Bmatrix} A \\ B \end{Bmatrix} = -\left[\begin{Bmatrix} \dot{Y}(x,t) \\ \vdots \\ \dot{Y}(x,t-\tau) \end{Bmatrix}, \begin{Bmatrix} Y(x,t) \\ \vdots \\ Y(x,t-\tau) \end{Bmatrix}\right]^{+} \begin{Bmatrix} \ddot{Y}(x,t) \\ \vdots \\ \ddot{Y}(x,t-\tau) \end{Bmatrix}, \tag{18}$$

where $(+)$ stands for the pseudo-inversion of the rectangular time discretized matrix $[\{\dot{Y}\},\{Y\}]$. Then, the equivalent frequency and damping parameters of the 1-dof fit to the nonlinear data are

$$\bar{f}_r = \sqrt{B}/(2\pi); \quad \bar{\zeta}_r = A/(4\pi\bar{f}_r). \tag{19}$$

All the methods discussed introduce a short time delay, of order $\tau/2$, in the frequency estimate. The choice of τ is a trade-off between the reliability of the frequency estimate, which increases with τ, and the tolerated latency $\tau/2$ of the estimate. For the purpose of the present study, a value of the order $\tau \sim 1/f_1$ was found adequate. Also note – and this is a point often overlooked or insufficiently stressed in the literature – that the "instantaneous" response frequency of the nonlinearly vibrating tube is actually a *local* property. For multi-supported tubes, irrespective of the technique used to estimate $\bar{f}_r(x,t)$, response frequencies computed near the loose supports are significantly higher than near midspans. This is because, near x_C, the vibratory responses are dominated by a local rattling behavior of the tube, meaning that the contribution of higher order modes is comparatively much higher there than near midspans. Therefore, except for very short tubes, one should not use a single value of $\langle \bar{f}_r(t) \rangle$ for the complete system, but compute $\bar{f}_r(x,t)$ along the tube. This leads to different reduced velocities $V_R(x,t)$, hence different coefficients $D_F(V_R(x,t))$ and $K_F(V_R(x,t))$ along the tube, which are then properly weighted according to Eq. (10).

2.6. Numerical simulations of the loosely supported tube

The method described in the previous section was used to simulate the nonlinear dynamical responses of a clamped-free flexible test tube, within a rigid square bundle, which is excited by the turbulence of a uniform transverse flow and subjected to fluidelastic coupling. The modeled tube has a length subjected to cross-flow $L_f=300$ mm and external diameter $D=30$ mm. At half length, a loose support is modeled using two opposite springs with stiffnesses $K_C=10^6$ N/m, this value having been adjusted in order to reproduce the experimental elemental tube/support spike contact time ($t_C=2\times10^{-3}s$). As a result of the clamping fixture, the tube motions are constrained to be planar, along the lift direction. Three different support configurations have been simulated: (a) with no loose support (for linear responses); (b) with a symmetrical loose support $\delta_C=\pm0.5$ mm and (c) with $\delta_C=\pm1$ mm. Because the test tube is quite short ($L/D=10$), the main contribution for the vibratory responses is from the first mode. Therefore, in the specific case of the present experiments, the dominant response frequency is mostly the same irrespective of the tube coordinate, hence $\langle\bar{f}_r(t)\rangle\simeq\bar{f}_r(x,t)$, $\forall x$. Ten modes, with frequencies in the range $f_n\approx18$ Hz$\sim$10 kHz (in stagnant water), were used for the nonlinear computations. Numerical integration of the nonlinear formulation (3)–(14) is achieved using an explicit method, based on the analytical solution of the modal equations in state-space (first order) form, with constant acceleration assumed within the time step (Hart and Wong, 1999). Simulations were performed for a total time of 40 s. An illustrative typical result obtained from the previously described techniques in shown in Fig. 1. Notice how, as expected, the estimate of the "instantaneous" frequency $\langle\bar{f}_r(t)\rangle$, computed from (18) and (19), increases significantly when the tube impacts.

3. Experimental rig and test procedures

The test rig is shown in Figs. 2–4. It is, essentially, the one used by Caillaud et al. (1999, 2000, 2003) in their tests, however a new instrumented tube with quite different modal frequency was used in the present experiments. Furthermore, the present experiments were designed for flow excited vibro-impacting on an instrumented loose support. The flexible steel tube, with the previously stated length L_f and diameter D, has a thin wall $e=0.5$ mm, being relatively light when compared with the added mass from the external fluid. The tube is clamped through a flat bar of length 100 mm, in order to constrain the vibrations to be planar, as shown in Fig. 2. The dimensions of the clamping bar are 100 mm $\times$ 25 mm $\times$ 4 mm, leading to a first modal frequency along the lift direction of 31 Hz in air, the corresponding value along the drag direction being about six times higher. This tube is the central one of a 3×5 square bundle of rigid tubes with reduced pitch $P/D=1.5$ (plus two columns of 5 half tubes at the boundaries). The first modal frequency of the rigid tubes lay beyond 1 kHz, two orders of magnitude higher than the first modal frequency of the flexible tube.

A single-phase water flow is imposed along the vertical direction, with pitch velocity in the range $V=0$–4 m/s. Measurement of the tube dynamical displacement, along the lift (horizontal) direction, was provided by a Zimmer camera OHG-100A, pointed toward the end of the tube. As shown in Figs. 2 and 3, for the nonlinear tests, two instrumented gap

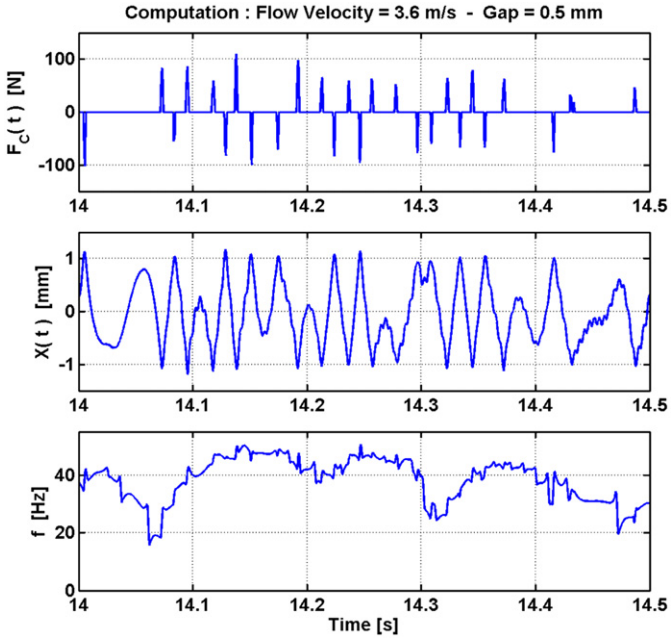

Fig. 1. Illustrative vibro-impact computation and estimate of the "instantaneous" response frequency.

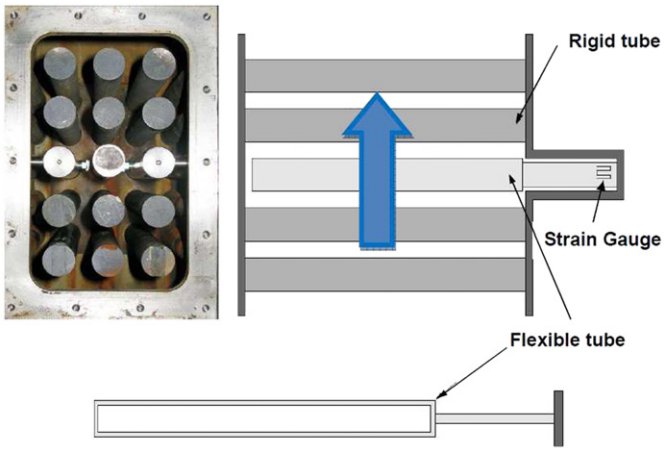

Fig. 2. Experimental rig with a flexible cantilever tube within a rigid bundle.

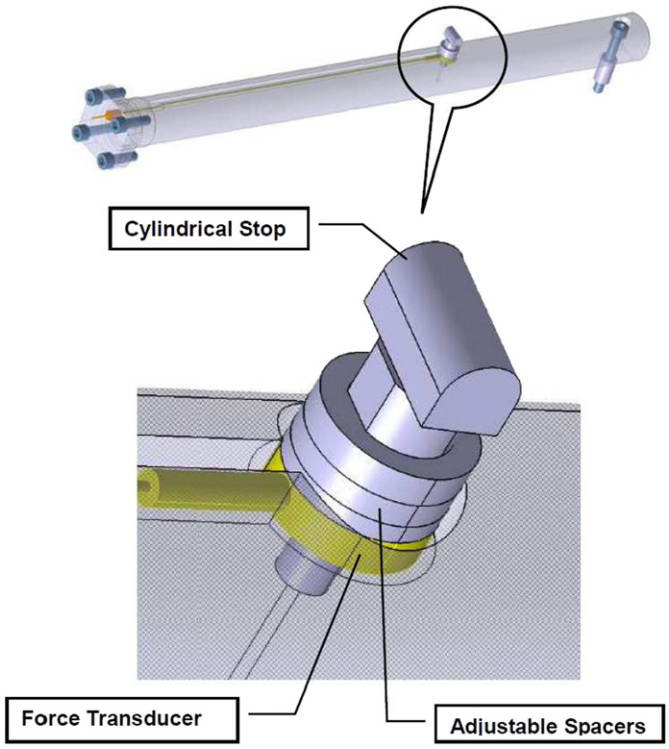

Fig. 3. Detail of one of the instrumented impact stops mounted on the neighboring rigid tubes.

stops were located symmetrically at the tube half length. The impact force measurements were performed by two piezoelectric force transducers Kistler 9132A. The gaps were conveniently adjusted using sets of spacers, as detailed in Fig. 3.

The first tests, performed under linear conditions (no loose support), were intended for the experimental identification of the fluidelastic coupling coefficients $C_d(V_R)$ and $C_k(V_R)$, the added mass C_m being assumed independent of the flow velocity. In order to explore the full range of experimental reduced velocity – well beyond the fluidelastic stability boundary of the "normal" system – the analog feedback stabilization technique used by Caillaud et al. (1999, 2000, 2003) has been adopted. It is, essentially, the one used earlier by Antunes et al. (1992) in their feedback controlled instability tests, but with reversed polarity. As implemented in the present experiments at CEA, the flexible tube was fitted with an accelerometer Endevco 2222C, located near the node of the tube second mode, whose response signal was electronically time integrated and amplified, being then fed to the electromechanical shaker shown in Fig. 4. A negative feedback loop was thus created, enabling a higher value of the tube first mode damping, which was controlled through the gain of the

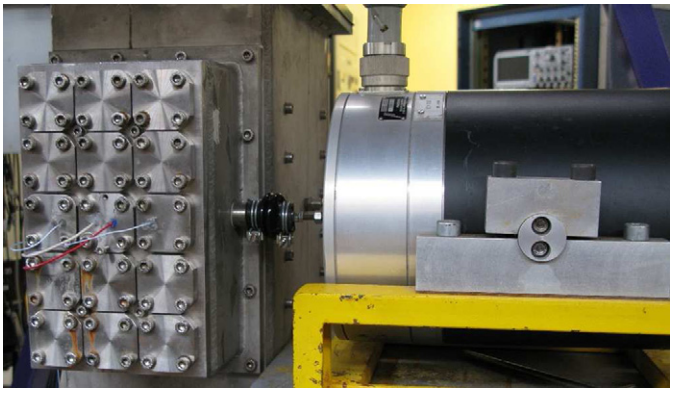

Fig. 4. Electromagnetic shaker for feedback control of the tube damping and stabilization.

power amplifier. Note that, due to the filtering used in the feedback loop to avoid undue modal spillover, the control force was not exactly in phase with the tube velocity. As a result, some residual feedback also affected the stiffness term, resulting in a change of the controlled tube modal frequency. This effect was carefully corrected when extracting the flow coupling coefficients from the identified modal parameters.

This control system enabled us to identify the fluidelastic coefficients in the range $V=0.5$–2.5 m/s, corresponding to a reduced velocity of about $V_R=1$–5 and a Reynolds number $\mathrm{Re}=7500\sim37500$, beyond which even the feedback loop was unable to cope with the fluidelastic destabilizing forces. However, for the vibro-impact tests, which were performed for two values of the support clearances, $\delta_C=\pm0.5$ mm and $\delta_C=\pm1$ mm, the full velocity range $V=0.5$–4 m/s was explored. These relatively large values of the gaps were chosen in order to emphasize the fluidelastic coupling forces. It should be noted that the ranges of Reynolds number and response frequencies explored in the present tests are quite different from those in the experiments by Tanaka and Takahara (1981) and Chen et al. (1998). For instance, in their tests Chen et al. stay within $\mathrm{Re}<4500$ and $V<0.2$ m/s, using excitation frequencies in the range 0.2–2 Hz. All these values are one order of magnitude lower than those of the present experiments.

4. Fluidelastic and turbulence forces from the transverse flow

4.1. Identified fluidelastic force coefficients

Because the added mass C_m is assumed independent of the flow velocity, the inertia coupling by the flow is trivially obtained by comparing the modal frequencies in air and in stagnant fluid, 31 Hz and 18 Hz, respectively, for the first mode. Similarly, the viscous fluid damping coefficient $C_d(0)$ at zero velocity can be inferred from the modal damping values in air and in stagnant fluid, 0.33% and 0.92%, respectively. The corresponding values of the modal mass, for the first mode, were found to be 0.066 and 0.16 kg (with modeshapes normalized such that $\max[|\varphi_n(0\leq x\leq L)|]=1$). Notice that the added mass from the external fluid almost triples the modal mass of the tube. On the other hand, the viscous damping results obtained were found to be consistent with the semi-empirical formulation proposed by Rogers et al. (1984).

Application of the general formulation (11) to the present system has shown that the incidence of the fluidelastic forces on the tube higher order modes is negligible. Therefore, under flow conditions, the fluidelastic coupling coefficients $C_k(V_R)$ and $C_d(V_R)$ are also easily inferred from the identified first modal frequency $f_1(V_R)$ and damping value $\zeta_1(V_R)$, accounting for the added damping from the stabilizing feedback loop, see Caillaud et al. (1999) for details.

The modal parameters, identified from the system response to the flow turbulence, are shown in Fig. 5 as a function of the flow velocity V. The fluidelastic coefficients obtained are shown in Fig. 6 as a function of the reduced velocity V_R. Notice in Fig. 5 the increase in damping, and decrease in the modal frequency, when the stabilizing feedback loop is closed. In accordance with Eq. (9), the sign convention for the fluidelastic coefficients plotted in Fig. 6 is such that positive values of $C_k(V_R)$ would increase the modal frequency of the flow/structure coupled system. Similarly, positive values of $C_d(V_R)$ are stabilizing.

Notice that, for the full range of flow velocity explored in the tests, $C_k(V_R)$ is negative, although its magnitude decreases as V_R increases. More importantly, as a general trend $C_d(V_R)$ decreases as V_R increases, clearly becoming negative and leading to fluidelastic instability beyond about $V_R>3.8$. Also notice the sudden decrease of C_d near $V_R\approx2.2$, a behavior that can be attributed to vortex shedding phenomenon.

4.2. Identified turbulence excitation

Using linear theory, see Axisa et al. (1990) for details, the authors identified the amplitude of the turbulence excitation spectrum from the vibratory response of the tube first mode, as the flow velocity was increased. The dimensionless results

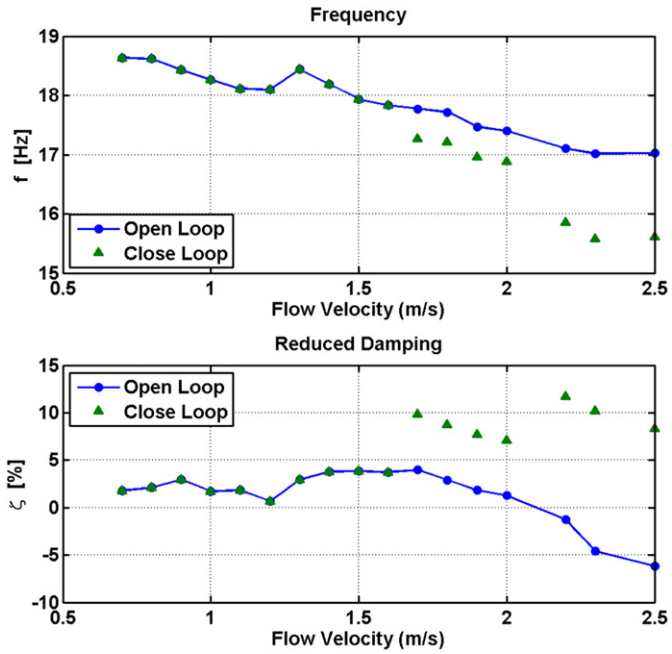

Fig. 5. Identified modal frequency and damping of the first tube mode as a function of the flow velocity (open loop: stabilizing feedback off; closed loop: stabilizing feedback on).

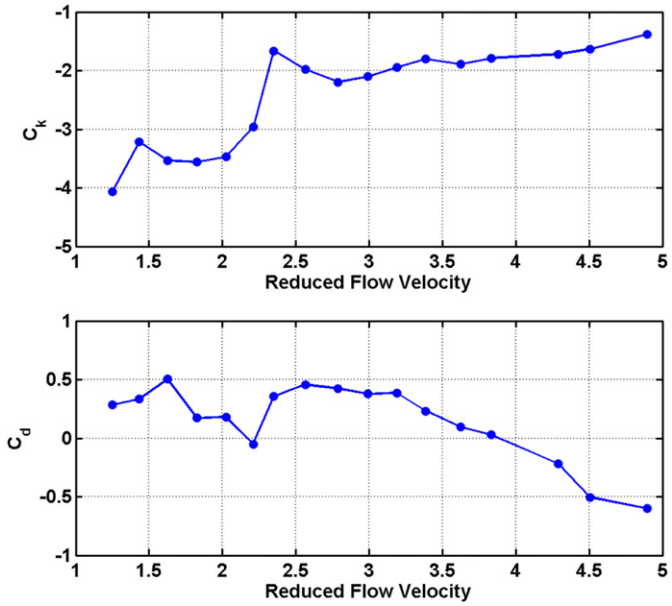

Fig. 6. Identified dimensionless fluidelastic coupling coefficients as a function of the reduced flow velocity.

thus obtained are shown in Fig. 7, as a function of the reduced frequency f_R, and they are plotted superimposed with the reference spectrum $[\Phi]_e(f_R)$ proposed as a design guideline by Axisa et al. (1990). One can notice that the agreement between the proposed reference spectrum and the present experimental data is nearly perfect.

5. Computational and experimental linear vibratory responses

Before tackling the nonlinear part of this work, the linear experimental results have been compared to the authors numerical simulation program, which was developed following the theoretical approach discussed in Section 2. Fig. 8 illustrates the first four modeshapes of the modal basis used in the numerical simulations, which were computed using

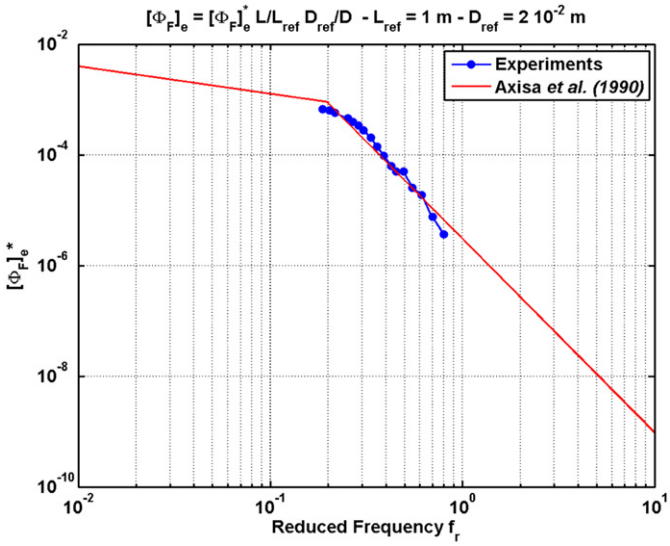

Fig. 7. Identified excitation data, superimposed to the equivalent reference spectrum of the turbulence forces per unit tube length proposed by Axisa et al. (1990).

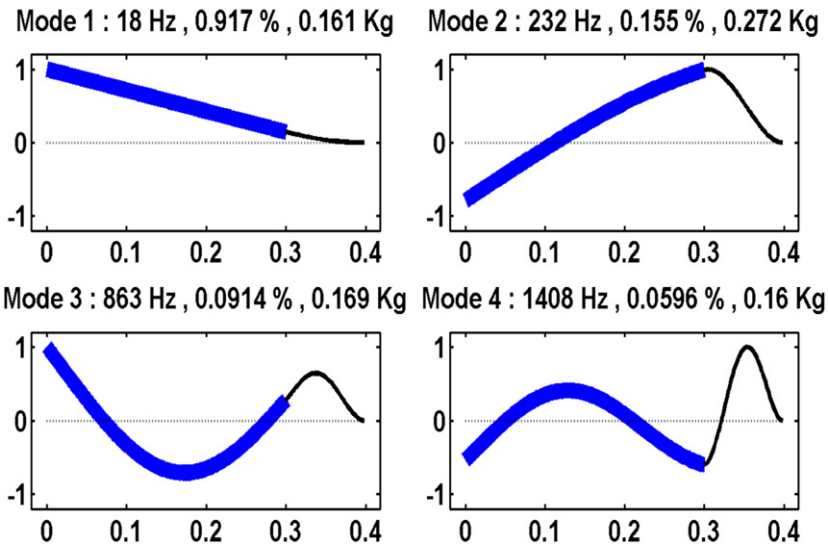

Fig. 8. First modes of the modal basis used in the time domain numerical simulations.

a finite element model. The modal frequencies and damping values used in the computations are those experimentally identified in still water. Notice that, because the tested tube is clamped to the wall through a flat bar, one should not expect the experimental modal frequencies to display the typical ratios of a common clamped-free tube.

The experimentally identified fluidelastic coefficients are used in the computations. First, the tube response frequency $\bar{f}_r(t)$ is estimated at each time step according to (18) and (19), from which the reduced velocity $V_R(t)$ is computed, which enables the interpolation of $C_k(V_R)$ and $C_d(V_R)$ from the experimental data of Fig. 6. Concerning turbulence excitation, the perfect agreement between the present experimental data and the excitation spectrum proposed by Axisa et al. (1990) enables us to use the spectrum of Fig. 7 in total confidence.

The perfect agreement of the results shown in Fig. 9 documents the overall coherence between the experimentally identified fluidelastic coefficients and their implementation in the computational tool. Plotted in the figure are the tube modal frequency $f_1(V)$ and damping $\zeta_1(V)$, under linear conditions, as a function of the flow velocity. Contrary to most of the data presented elsewhere in the paper, the results shown here were not directly extracted from time domain responses, but obtained using frequency-domain techniques, namely, the data points labeled "Experiments" pertain to the experimental identification of the tube modal parameters using a SDOF identification algorithm, from which the experimental fluidelastic coefficients $C_k(V_R)$ and $C_d(V_R)$ were inferred. The data points labeled "Computations" are obtained

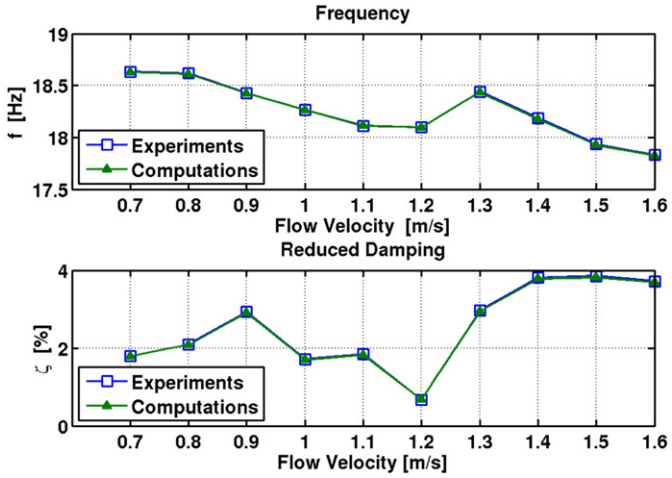

Fig. 9. Comparison between the measured modal parameters and those computed from the identified fluidelastic coefficients.

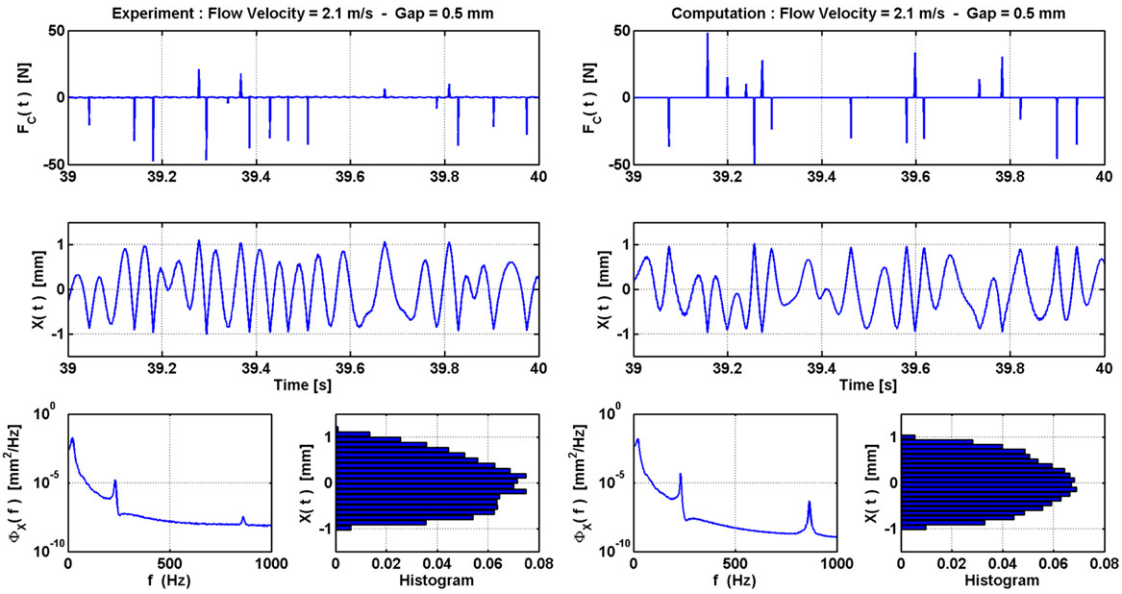

Fig. 10. Comparison between the measured and computed responses at velocity $V=2.1$ m/s with a gap $\delta_c=\pm 0.5$ mm.

from a complex eigenvalue analysis of the flow coupled tube, after the fluidelastic coefficients were implemented in formulation (11). These preliminary computations were followed by the time domain numerical simulations in all the subsequent work.

6. Computational and experimental vibro-impact responses

6.1. Detailed experimental and computed responses

The final and the most important aspect of this work is now addressed, namely, asserting if the fluidelastic coefficients obtained under steady oscillatory conditions may be used with confidence when modeling the unsteady nonlinear dynamics of vibro-impacting flow excited tubes. First, the results obtained are illustrated by showing detailed plots from experiments and computations at two different velocities and two values of the support gap. Then overall statistical results are presented, for the complete range of velocity explored, comparing the experimental and computed vibro-impact forces and the tube response frequencies.

Fig. 10 displays samples of the experimental and computed tube responses, for the flow velocity $V=2.1$ m/s with support gap $\delta_C=\pm 0.5$ mm. Fig. 11 presents the results obtained for $V=3.6$ m/s with $\delta_C=\pm 1$ mm. In these figures are shown plots of the impact force at x_C, the tube displacement response at the free end of the tube, the corresponding

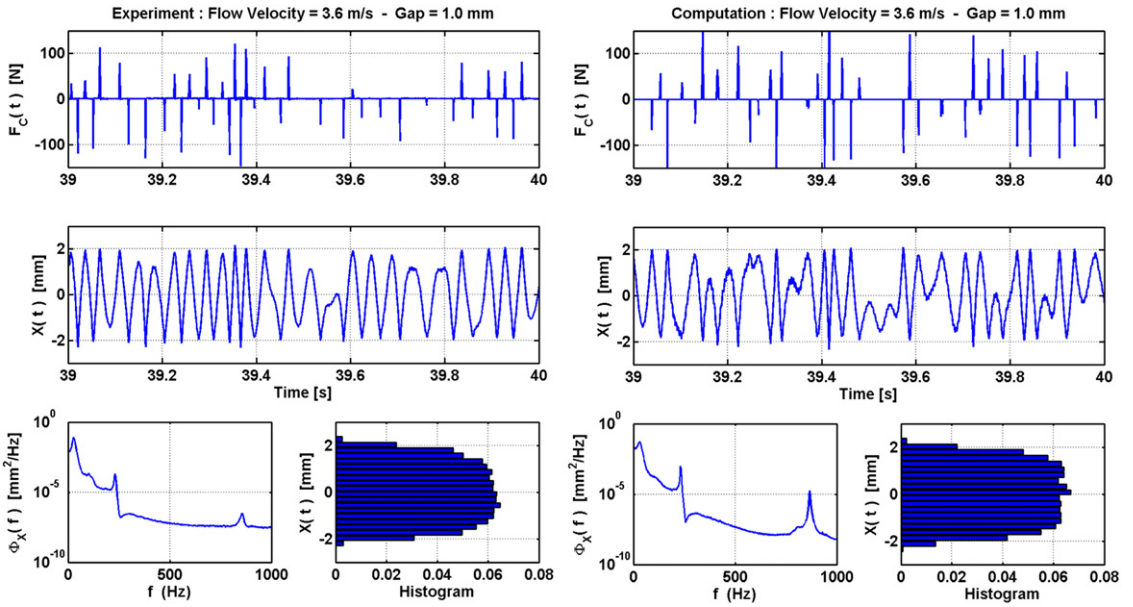

Fig. 11. Comparison between the measured and computed responses at velocity $V=3.6$ m/s with a gap $\delta_c=\pm 1$ mm.

response spectrum and amplitude histogram. Notice that the vibration amplitude is bounded at about the double of the gap δ_C at location $L/2$, as can be understood from the first modeshape in Fig. 8.

The results shown in Fig. 10, at velocity $V=2.1$ m/s ($V_R=3.4$), almost at the verge of fluidelastic instability. The support gap $\delta_C=\pm 0.5$ mm is small enough for relatively intense impacting, as a result of the turbulence forces. Notice the good agreement between all features of the experimental and the computed responses, the sole differences concerning the higher order modal spectral responses, which appear more damped in the experiments.

Results in Fig. 11 concern the higher velocity $V=3.6$ m/s, which induces a severe fluidelastically unstable system, using the larger support gap $\delta_C=\pm 1$ mm. A violently nonlinear vibro-impacting regime is now obtained, with a far from Gaussian tube response. This is due in part to the higher turbulence excitation, but mostly to the large destabilizing fluidelastic coupling forces, which, being proportional to the vibration amplitude, are enhanced by the larger support gap. Notice that, as before, the agreement between experiments and computations is very satisfying.

6.2. Global results and energy aspects

The method developed here for the estimation of the computational response frequency could not be used on the experimental results, because not all the response signals $Y(t)$, $\dot{Y}(t)$ and $\ddot{Y}(t)$ – used in Eq. (18) – were available in the measurements. Obviously, from the measured displacement, the velocity and acceleration could be derived, but at the cost of some noise amplification. The authors decided this was a good reason to compare the response frequencies $\bar{f}_r$ predicted by their algorithm with a different method better suited to deal with the experimental results. Fig. 12 shows the results obtained for the average response frequency, by processing the total length of the computed responses with Rice's formula (15) (hence with σ_Y and $\sigma_{\dot{Y}}$ computed from the total signals) and with the time averaged value obtained from the equivalent 1-dof oscillator method. It appears that, except at the lowest flow velocities when the system is linearly stable, both methods produce similar results, for all practical purposes. However, as seen from the plot with $\delta_C=\pm 0.5$ mm, at the lowest flow velocities $V\leq 1.1$ m/s, where the tube does not impact, the 1-dof oscillator method consistently extracts the correct modal frequency of the first mode (18 Hz) from the random response, while Rice's formula leads to lower incorrect values.

In Figs. 13 and 14, a comparison between the experimental and computational results is presented, for the complete range of flow velocity explored, and for the two support gaps tested. Fig. 13 shows a quantifier (among other possible options) of the impact force magnitude—the average of the impact force maxima. For $\delta_C=\pm 0.5$ mm, no impacts are displayed by the linearly stable system up to $V\approx 1$ m/s, this velocity being increased to $V\approx 1.5$ m/s for the larger gap $\delta_C=\pm 1$ mm. Then, the impact forces magnitudes increase steadily with the flow velocity. All qualitative features of the experimental results are perfectly reproduced by the computations, including the velocity boundaries where the tube starts to impact. Quantitatively, one may notice that the computed impact forces at higher flow velocities are about 20% higher than the corresponding experimental forces. This difference might be due to the fact that in the computations the impact damping at the loose support was neglected, or to a possible underestimation of the higher-order modal damping values. These aspects deserve to be further investigated.

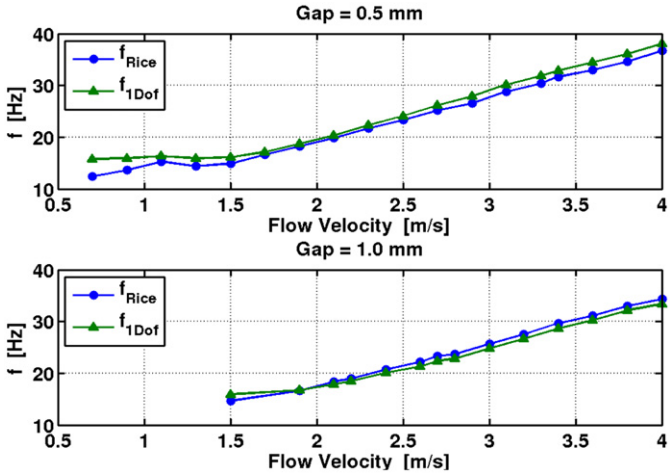

Fig. 12. Comparison between the computed response frequencies estimated using Rice's formula and the equivalent 1-dof oscillator technique.

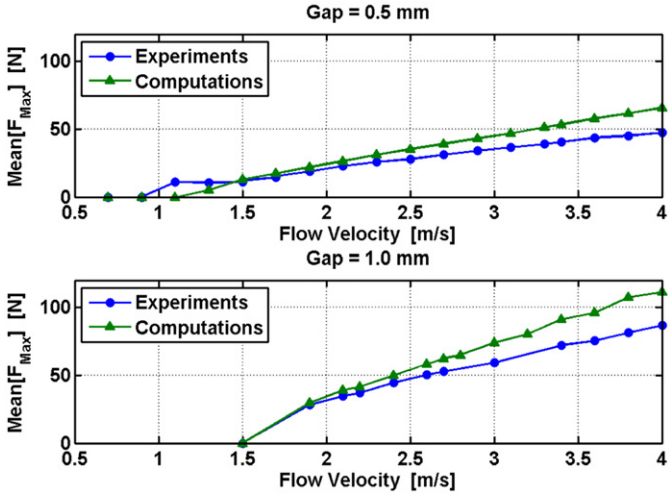

Fig. 13. Comparison between the tube experimental and computed impact forces.

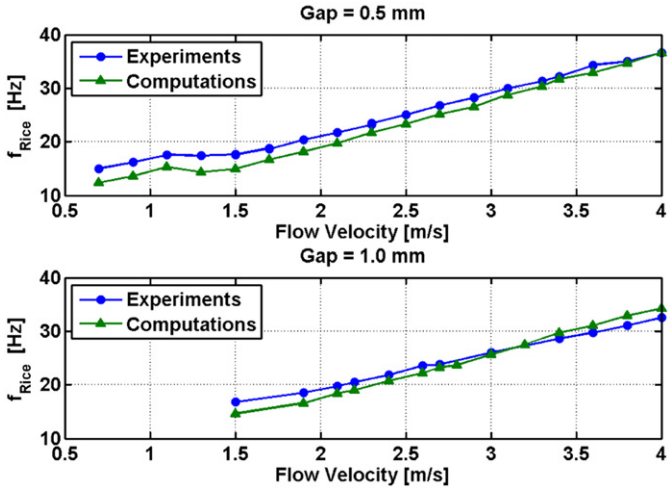

Fig. 14. Comparison between the tube experimental and computed response frequencies.

Concerning the effect of the support gap on the magnitude of the impact forces, notice that, as soon as the system becomes linearly unstable, higher impact forces are observed on the larger gap system. This is simply because, although they also depend on the response frequency, the fluidelastic forces are essentially proportional to the system vibratory amplitude and hence, beyond instability, increase almost proportionally with δ_C.

In Fig. 14 the experimental and computational response frequencies of the system (both estimated according to Rice's formula) are presented and, again, their comparison is highly satisfactory. At low velocities, when the system is not impacting, the time domain frequency responses are those of the flow coupled first mode. Then, beyond the instability boundary, the system experiences a steady increase of $\bar{f}_{Rice}$ with the flow velocity. This result is a direct consequence of an increase in the system effective stiffness, connected with increasingly intense vibro-impact dynamical regimes.

The quite good agreement between the nonlinear experimental and computational results shown in Figs. 13 and 14 enables us to conclude that, in spite of having obtained the fluidelastic coefficients $C_k(V_R)$ and $C_d(V_R)$ under steady oscillatory conditions, it appears quite satisfactory to use them for performing severely nonlinear unsteady computations.

In Fig. 15 the average values of the reduced velocities obtained from the nonlinear experiments and computations are plotted as a function of the flow velocity. Recall that V_R only increases proportionally to V under linear conditions. For vibro-impacting systems their relationship is not straightforward, because the actual response frequency $\bar{f}_r$ used in $V_R = V/\bar{f}_r D$ is not constant, being dependent on the (a priori unknown) response regime of the nonlinear system. Having this in mind, the dynamical behavior of loosely supported tubes subjected to fluidelastic forces is well clarified by Fig. 15. It appears that, beyond the linear instability boundary – and at least for a large range of flow velocity – the system dynamics self-regulate in order to produce a mean response frequency, which leads to an almost constant value of the reduced velocity.

The meaning of this is partly clarified by noting that the "asymptotic" value $V_R^* \approx 4$ in the plots of Fig. 15 is the reduced velocity at which the coupling coefficient $C_d(V_R)$ changes from positive to negative, see Fig. 6. Therefore, for a given flow velocity $V > V_{crit}$, the linearly unstable vibro-impacting system will increase its response frequency up to a mean value $\bar{f}_r^*$ such that the effective *average* damping of the flow coupled system becomes almost zero, hence $C_d(V_R^*) \approx 0$, which implies $V_R^* \approx 4$. This is the simple condition, which enables a viable energy balance for this system, in which instability is controlled by damping. For flexible tube bundles, which may become linearly unstable through damping and stiffness mechanisms, the conditions, which define the nonlinear response regimes "chosen" by the system, are possibly more involved. However, in the authors' opinion, the same principle should apply.

As a side point notice that, because the vibro-impacting system never "allows" average reduced velocities higher than $V_R^* \approx 4$, we may achieve credible nonlinear computations at flow velocities higher than those where the fluidelastic coefficients of the linear system were identified.

The general discussion of Fig. 15 neglects the important role of the turbulence forces and will be now supplemented by the detailed information provided by the plots in Fig. 16. The values of the average power components related to (a) the structural dissipation, (b) the fluidelastic coupling forces and (c) the turbulence forces, which are shown in the plots, were computed from the results of the numerical simulations as follows, in terms of the modal parameters and the modal force components and velocities defined in Eqs. (2) and (4):

$$\langle P_\zeta \text{ Tube} \rangle = \frac{1}{T}\int_0^T \left(\sum_{n=1}^{N} 2m_n \omega_n \zeta_n [\dot{q}_n(t)]^2 \right) dt, \tag{20}$$

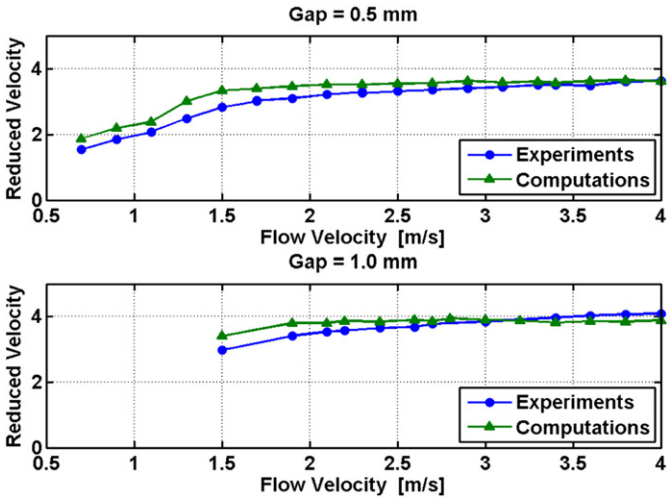

Fig. 15. Comparison between the tube experimental and computed average reduced velocities as a function of the flow velocity.

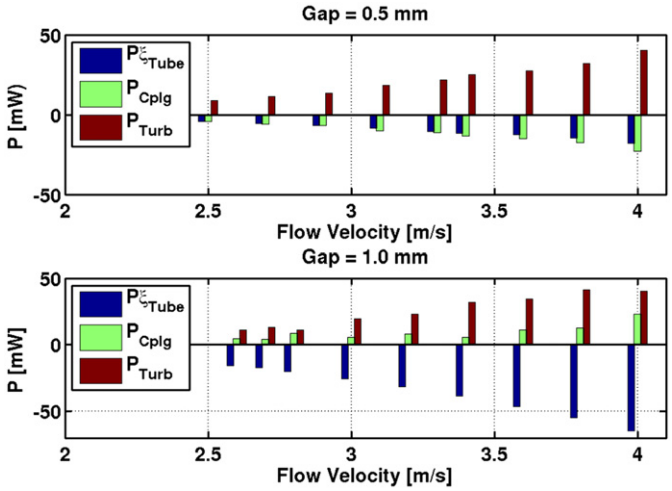

Fig. 16. Computed energy terms as a function of the flow velocity and support gap.

$$\langle P_{\mathrm{Cplg}} \rangle = \frac{1}{T}\int_0^T \left(\sum_{n=1}^{N} F_n^F(t)\dot{q}_n(t)\right)dt, \tag{21}$$

$$\langle P_{\mathrm{Turb}} \rangle = \frac{1}{T}\int_0^T \left(\sum_{n=1}^{N} F_n^T(t)\dot{q}_n(t)\right)dt. \tag{22}$$

These values quantify the energy "paths" in the system, for increasing values of the flow velocity and for the two support gaps addressed. Positive values indicate that energy is supplied to the tube, while negative values indicate dissipated energy. As expected, turbulence forces always supply energy and the structural damping is always dissipative.

The most interesting part in these plots relates to the energy behavior stemming from the fluidelastic coupling terms. For the smaller gap system, as a result of the gap limited motion amplitude and accounting for the tube mean response frequency, it appears that the time averaged fluidelastic forces associated with the nonlinear vibro-impact regime are of dissipative nature, irrespective of the flow velocity. In other words, the "active" vibration source is the flow turbulence. However, for the larger gap system, the scenario is quite different, because at higher velocities the fluidelastic forces become destabilizing. In this case, the energy input is shared by both the turbulence and the fluidelastic forces. These interesting results, for which the authors tentatively provide the mentioned view, deserve a closer look in the future, based on a thorough analysis of the computational data.

7. Conclusions

In this paper the authors presented experimental and computational results, which constitute an overall validation of their approach to deal with loosely supported tubes subjected to fluidelastic forces and flow turbulence excitation. The main point addressed was to assert the validity of computing the nonlinear and unsteady vibro-impact responses of fluidelastically unstable tubes, knowing that the fluidelastic coupling coefficients are typically provided by tests performed under steady oscillatory conditions. The system studied here was constrained to planar motions in the lift direction, leading to normal impact forces only. In spite of their importance, the authors did not address friction and wear related effects, which would stem from two-dimensional tube vibrations, because such aspects were not of prime interest in this work.

The results obtained clearly suggest that the modeling approach developed is consistent with the nonlinear experiments, and therefore reliable. Because the authors' general modeling framework is shared by other researchers, they may also feel reassured by the present investigation.

Among other aspects developed in this work, several techniques were reviewed for estimation of the "instantaneous" response frequency of nonlinear regimes. A new simple and reliable method, well suited for the nonlinear computations, was proposed and applied.

New experimental identifications of the fluidelastic coefficients were performed, using a feedback stabilizing technique, which allows for identifications at high flow velocities. The experimental coefficients, obtained on a flexible tube within a rigid tube bundle with $P/D=1.5$, corroborate those previously obtained by Caillaud et al. (1999). On the other hand, the turbulence excitation spectrum for the rig tested was identified, leading to results, which lay perfectly on the reference spectrum recommended by Axisa et al. (1990).

Finally, under nonlinear conditions, extensive experiments and computations were performed, for a large range of flow velocity and two values of the tube support gap. Beyond providing a global validation of the authors' modeling approach,

the results obtained offer interesting insights on the nonlinear behavior of the tube. In particular, it became clear how the average response frequency is established by the vibro-impacting system. On the other hand, the analysis of the results provided by the two support gaps tested highlights possible scenarios, which may arise, with respect to the various terms involved in an energy balance of the flow excited tube.

Acknowledgments

The authors acknowledge financial support for this work, which was performed in the framework of a joint research program cofunded by AREVA NP, EDF and CEA (France). Also, concerning the experimental part of this paper, the valuable contribution of Thierry Valin from CEA/DEN/DM2S/SEMT/DYN (Saclay, France) is acknowledged. Finally, the thorough comments and criticisms of the original manuscript, which were provided by the anonymous reviewers, are gratefully acknowledged.

References

Antunes, J., Axisa, F., Beaufils, B., Guilbaud, D., 1990. Coulomb friction modelling in numerical simulations of vibration and wear work rate of multi-span heat-exchangers. Journal of Fluids and Structures 4, 287–304.

Antunes, J., Axisa, F., Vento, M.A., 1992. Experiments on tube-support interaction with feedback controlled instability. ASME Journal of Pressure Vessel Technology 114, 23–32.

Antunes, J., Delaune, X., Piteau, P., Borsoi, L., 2008. A simple consistent method for the time-domain simulation of turbulence excitations applied to tube/support dynamical analysis under non-uniform flows. In: Proceedings of the 9th International Conference on Flow Induced Vibrations (FIV-2008), Prague, Czech Republic, 30 June–3 July 2008.

Antunes, J., Piteau, P., Delaune, X., Borsoi, L., 2009. An evaluation of methods for the time-domain simulation of turbulence excitations for tube bundles subjected to non-uniform flows. In: Proceedings of the 20th International Conference on Structural Mechanics in Reactor Technology (SMIRT 20), Espoo, Finland, 9–14 August 2009.

Au-Yang, M.K., 2002. The crossing frequency as a measure of heat exchanger support-plate effectiveness. Journal of Fluids and Structures 16, 83–92.

Axisa, F., Antunes, J., Villard, B., 1988. Overview of numerical methods for predicting flow-induced vibration. ASME Journal of Pressure Vessel Technology 110, 6–14.

Axisa, F., Antunes, J., Villard, B., 1990. Random excitation of heat-exchanger tubes by cross-flow. Journal of Fluids and Structures 4, 321–341.

Boashash, B., 1992. Estimating and interpreting the instantaneous frequency of a signal—part 1: fundamentals; part 2: algorithms and applications. Proceedings of IEEE 80, 519–568.

Caillaud, S., de Langre, E., Piteau, P., 1999. The measurement of fluidelastic effects at low reduced velocities using piezoelectric actuators. ASME Journal of Pressure Vessel Technology 121, 232–238.

Caillaud, S., de Langre, E., Piteau, P., 2000. Measurement of critical velocities for fluidelastic instability using vibration control. ASME Journal of Vibration and Acoustics 122, 341–345.

Caillaud, S., de Langre, E., Baj, F., 2003. Active vibration control for the measurement of fluidelastic effects. ASME Journal of Pressure Vessel Technology 125, 165–170.

Chen, S.S., Cai, Y., Srikantiah, G.S., 1998. Fluid damping controlled instability of tubes in crossflow. Journal of Sound and Vibration 217, 883–907.

Connors, H.J., 1970. Fluidelastic vibration of tube arrays excited by cross-flow. In: Reiff, D.D. (Ed.), Proceedings on Flow-Induced Vibration in Heat-Exchangers, ASME, pp. 42–46.

De Araujo, M., Antunes, J., Piteau, P., 1998. Remote identification of impact forces on loosely supported tubes : part 1—basic theory and experiments. Journal of Sound and Vibration 215, 1015–1041.

Fricker, A., 1992. Numerical analysis of the fluid-elastic vibration of a steam generator tube with loose support. Journal of Fluids and Structures 6, 85–107.

Granger, S., Campistron, R., Lebret, J., 1993. Motion-dependent excitation mechanisms in a square in-line tube bundle subject to water cross-flow: an experimental modal analysis. Journal of Fluids and Structures 7, 521–550.

Hadj-Sadok, C., Payen, T., de Langre, E., 1997. Modelling of fluidelastic vibrations of heat exchanger tubes with loose supports. In: Proceedings of the 4th International Symposium on Fluid-Structure Interaction, Aeroelasticity and Flow-Induced Vibration and Noise, Dallas, USA 53-2, 16–21 November 1997, pp. 193–199.

Hart, G.C., Wong, K., 1999. Structural Dynamics for Structural Engineers. John Wiley & Sons, New York, USA.

Hassan, M., Hayder, M., 2008. Nonlinear vibrations of loosely supported tubes excited by fluidelastic and turbulence forces. Nuclear Engineering and Design 238, 2507–2520.

Hassan, M.A., Weaver, D.S., Dokainish, M.A., 2005. A new tube/support impact model for heat exchanger tubes. Journal of Fluids and Structures 21, 561–577.

Inada, F., Nishihara, T., Yasuo, A., Morita, R., Sakashita, A., Mizutani, J., 2003. Self-excited vibration of cross-shaped tube bundle in cross-flow. Journal of Fluids and Structures 18, 651–661.

Lever, J.H., Weaver, D.S., 1982. A theoretical model for the fluidelastic instability in heat exchanger tube bundles. ASME Journal of Pressure Vessel Technology 104, 147–158.

Mitra, D., Dhir, V.K., Catton, I., 2009. Fluid-elastic instability in tube arrays subjected to air–water and steam–water cross-flow. Journal of Fluids and Structures 25, 1213–1235.

Mureithi, N., Ito, T., Nakamura, T., 1996. Identification of fluidelastic instability under conditions of turbulence and nonlinear tube supports. In: Proceedings of the ASME Pressure Vessel and Piping Conference, Montreal, Canada, ASME PVP-328, pp. 19–24.

Pachet, F., Briot, J.P. (Eds.), 2004. Informatique Musicale: du Signal au Signe Musical. Hermès Science Publications, Paris, France (Chapter 1).

Rao M.S., Steininger D.A., Ahluwalia, K.S., Eisinger F.L., 1992. Simulation of PWR steam generator tubes undergoing turbulence and fluidelastic excitation for wear prediction. In: Proceedings of the ASME International Symposium on Flow-Induced Vibrations and Noise, Anaheim, USA, vol. 230, pp. 185–210.

Rice, S.O., 1945. Mathematical analysis of random noise. Bell System Technical Journal 24, 46–156.

Rogers, R.J., Taylor, C., Pettigrew, M.J., 1984. Fluid effects on multispan heat-exchanger tube vibration. In: Proceedings of the ASME Pressure Vessel and Piping Conference, San Antonio, USA.

Sauvé, R.G., 1996. A computational time domain approach to fluidelastic instability for nonlinear tube dynamics. In: Proceedings of the Symposium on Flow-Induced Vibrations, Montreal, Canada, ASME PVP/ICPVT-8, pp. 111–121.

Tanaka, H., Takahara, S., 1981. Fluidelastic vibration of tube arrays in cross-flow. Journal of Sound and Vibration 77, 19–37.

Vento, M.A., Antunes, J., Axisa, F., 1992. Tube/support interaction under simulated fluidelastic instability: two-dimensional experiments and computations of the nonlinear responses of a straight tube. In: Proceedings of the Symposium on Flow-Induced Vibration and Noise, Anaheim, USA, ASME PVP-242, pp. 151–166.